# Structural semiconductor-to-semimetal phase transition in two-dimensional materials induced by electrostatic gating

Yao Li[1], Karel-Alexander N. Duerloo[2], Kerry Wauson[3] & Evan J. Reed[2]

Dynamic control of conductivity and optical properties via atomic structure changes is of technological importance in information storage. Energy consumption considerations provide a driving force towards employing thin materials in devices. Monolayer transition metal dichalcogenides are nearly atomically thin materials that can exist in multiple crystal structures, each with distinct electrical properties. By developing new density functional-based methods, we discover that electrostatic gating device configurations have the potential to drive structural semiconductor-to-semimetal phase transitions in some monolayer transition metal dichalcogenides. Here we show that the semiconductor-to-semimetal phase transition in monolayer $MoTe_2$ can be driven by a gate voltage of several volts with appropriate choice of dielectric. We find that the transition gate voltage can be reduced arbitrarily by alloying, for example, for $Mo_xW_{1-x}Te_2$ monolayers. Our findings identify a new physical mechanism, not existing in bulk materials, to dynamically control structural phase transitions in two-dimensional materials, enabling potential applications in phase-change electronic devices.

[1] Department of Applied Physics, Stanford University, Stanford, California 94305, USA. [2] Department of Material Science and Engineering, Stanford University, Stanford, California 94305, USA. [3] Klipsch School of Electrical and Computer Engineering, New Mexico State University, Las Cruces, New Mexico 88003, USA. Correspondence and requests for materials should be addressed to E.J.R. (email: evanreed@stanford.edu).

Structural phase transitions yielding a change of electrical conductivity are a topic of long-standing interest and importance[1,2]. Two of the most studied phase-change material classes for electronic and optical applications are metal oxide materials[3,4] and GeSbTe alloys[5], both having a large electrical contrast. For example, the metal oxide material vanadium dioxide ($VO_2$) is reported to exhibit a structural metal–insulator transition near room temperature at ultrafast timescales, which can be triggered by various stimuli including heating[6], optical[7] excitations and strain[8]. GeSbTe alloys can undergo reversible switching between amorphous and crystalline states with different electrical resistivity and optical properties. This is usually achieved by Joule heating employed in phase-change memory applications[9,10]. These materials are distinguished from the myriad materials that exhibit atomic structural changes by the proximity of a phase boundary to ambient conditions.

Another group of materials that can undergo phase transitions are layered transition metal dichalcogenides (TMDs), which have received recent attention as single- and few-layer materials, although research on bulk TMDs dates back decades[11,12]. Early attention has been focused primarily on electronic transitions between incommensurate and commensurate charge density wave[13,14] phases and superconducting phases[15]. Some TMDs have been found to exist in multiple crystal structures[16], and transitions between them have been demonstrated in group V TMDs ($TaSe_2$ and $TaS_2$) utilizing an scanning tunnelling microscope (STM) tip[17,18]. These reported transitions in $TaSe_2$ and $TaS_2$ are between two metallic phases. Recently, group VI TMDs have attracted increasing attention because they can exist in a semiconducting phase[19]. Recent computational work indicates that structural transitions between phases of large electrical contrast in some exfoliated two-dimensional (2D) group VI TMDs can be driven by mechanical strain[20]. Excess charges transferred from chemical surroundings are also reported to induce structural phase transitions in 2D group VI TMDs[21–24]. One would like to know the threshold charge density required to induce these transitions and whether these transitions could be dynamically controlled by electrostatic gating, utilizing standard electronic devices.

Here we show the potential of phase control in some monolayer TMDs using electrostatic gating device configurations. In this work, we use density functional theory (DFT) to determine the phase boundaries of single-layer $MoS_2$, $MoTe_2$, $TaSe_2$ and the alloy $Mo_xW_{1-x}Te_2$. We consider $MoS_2$ because it has received considerable attention as an exceptionally stable semiconductor, and $MoTe_2$ because DFT calculations indicate that its energy difference between semiconducting and semimetallic phases is exceptionally small among Mo- and W-TMDs[20]. We calculate the phase boundaries at conditions of constant charge and constant voltage, the electrical analogues to mechanical conditions of constant volume and constant pressure, respectively. We find that a surface charge density of less than $-0.04\,e$ or greater than $0.09\,e$ per formula unit is required to observe the semiconductor-to-semimetal phase transition in undoped monolayer $MoTe_2$ under constant-stress conditions ($e$ is the elementary electric charge) and a much larger value of approximately $-0.29\,e$ or $0.35\,e$ per formula unit is required in the undoped monolayer $MoS_2$ case. The charge densities discussed in this work refer to excess charge density and should not be misinterpreted as the electron or hole density in a charge-neutral material that one might obtain from chemical doping. We also study the potential of phase control in monolayer $MoTe_2$ and $TaSe_2$ through electrostatic gating using a capacitor structure. We discover that a gate voltage as small as a few volts for some choices of gate dielectric can be applied to drive the phase transition in

monolayer $MoTe_2$ using a capacitor structure. While the required field magnitudes are large and may be challenging to achieve, we find that the transition gate voltage may be reduced to 0.3–1 V and potentially lower by substituting a specific fraction of W atoms within $MoTe_2$ monolayers to yield the alloy $Mo_xW_{1-x}Te_2$. To accomplish these calculations, we have developed a DFT-based model of the electrostatically gated structure (Supplementary Figs 1 and 2; Supplementary Note 1). This approach is validated by comparing to direct DFT simulations in Supplementary Fig. 3 and Supplementary Note 2.

## Results

**Crystal structures.** TMDs are a class of layered materials with the formula $MX_2$, where M is a transition metal atom and X is a chalcogen atom. Each monolayer is composed of a metal layer sandwiched between two chalcogenide layers, forming a X–M–X structure[16] that is three atoms thick. The weak interlayer attraction of TMDs allows exfoliation of these stable three-atom-thick layers. Given the crystal structures reported in the bulk, we expect that exfoliated monolayer TMDs have the potential to exist in the crystal structures shown in Fig. 1. Figure 1 shows the X atoms with trigonal prismatic coordination, octahedral coordination or a distorted octahedral coordination around the M atoms[16,20,25,26]. We will refer to these three structures of the monolayer as the 2H phase, 1T phase and 1T′ phase, respectively. Symmetry breaking in the 1T′ leads to a rectangular primitive unit cell.

Among these 2D TMDs, the Mo- and W-based materials have attracted the most attention because their 2H crystal structures are semiconductors with photon absorption gaps in the 1–2 eV (ref. 27) range, showing potential for applications in ultrathin flexible and nearly transparent 2D electronics. Radisavljevic et al.[28] fabricated single-layer $MoS_2$ transistors of high mobility, large current on/off ratios and low standby power dissipation. Unlike group IV and group V TMDs (for example, $TaSe_2$ and $TaS_2$), which have been observed in the metallic 1T crystal structure[16], DFT calculations on the group VI TMDs (Mo and W based) freestanding monolayers indicate that the 1T structure is unstable in the absence of external stabilizing influences[20]. However, group VI TMDs do have a stable octahedrally coordinated structure of large electrical conductivity, which is a distorted version of the 1T phase and referred to as 1T′ structure (Fig. 1). On the basis of DFT calculation results, Kohn–Sham
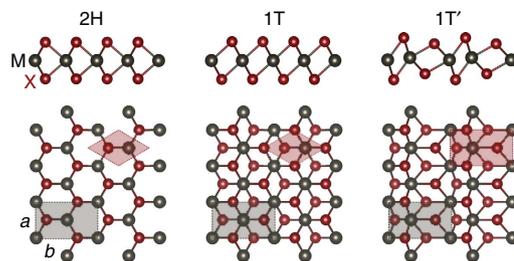


**Figure 1 | Three crystal structures of monolayer TMDs.** The top schematics show cross-sectional views and the bottom schematics show basal plane views. The grey atoms are transition metal atoms and the red atoms are chalcogen atoms; in all three phases, a layer of transition metal atoms (M) is sandwiched between two chalcogenide layers (X). The semiconducting 2H phase has trigonal prismatic structure, and the metallic 1T and semimetallic 1T′ phases have octahedral and distorted octahedral structures, respectively. The grey shadow represents a rectangular computational cell with dimensions $a \times b$, and the red shadow represents the primitive cell.

states of this 1T′ crystal structure have metallic or semimetallic characteristics, consistent with previous experiments[16]. This octahedral-like 1T′ crystal structure has been observed in $WTe_2$ under ambient conditions[16,29], in $MoTe_2$ at high temperature[29] and in lithium-intercalated $MoS_2$ (ref. 25). There is recent experimental evidence that few layer films of the T′ phase of $MoTe_2$ exhibit a bandgap that varies from 60 meV to zero with variations in number of layers[30].

The relative energies of Mo- and W-based TMDs monolayer crystals shown in Fig. 1 have been calculated using semilocal DFT with spin–orbit coupling, shown in Supplementary Fig. 4. These results are consistent with experimental evidence that the bulk form of $WTe_2$ is stable in the metallic 1T′ phase, while other Mo- and W-dichalcogenides are stable in the semiconducting 2H phase[16]. These calculations indicate that the switch from semiconducting 2H phase to semimetallic 1T′ phase in monolayer $MoTe_2$ requires the least energy (31 meV per formula unit), suggesting the potential for a transition that is exceptionally close to ambient conditions. Therefore, we choose to focus on determining the phase boundary of monolayer $MoTe_2$. While the computed energy difference between 2H and 1T′ is considerably larger for $MoS_2$ (548 meV per formula unit), we also compute phase boundaries for this monolayer at constant charge because it has received more attention in the laboratory to date. Among 2D group VI TMDs, monolayer $MoS_2$ has attracted the most experimental attention for its stability and relative ease of exfoliation and synthesis. Monolayer $MoTe_2$ has also been exfoliated[31,32] and its synthesis is a fast-developing field.

**Energy calculations for charged monolayers.** We examine two distinct thermodynamic constraints for a system containing a charged monolayer. In one scenario, the monolayer is constrained to be at constant excess charge, as shown in Fig. 2a; in the other, the monolayer is constrained to be at constant voltage, as shown in Fig. 2b. These are the electrical analogues to mechanical conditions of constant volume and constant pressure, respectively. The electrical contact depictions in Fig. 2b and subsequent figures are schematic and could be accomplished in other manners, for example, side contacts. In Fig. 2b, the charge is assumed to be stored in the monolayer rather than the metal contact. Layer I is a monolayer TMDs with a Fermi level $\mu_f^I$, and plate II has a Fermi level of $\mu_f^{II}$. A dielectric medium of thickness $d$ and capacitance $C$ is sandwiched between monolayer TMDs and plate II. This dielectric medium can be vacuum. Distance $s^I$ is the separation between the centre of monolayer TMDs I and the right surface of the dielectric medium, while $s^{II}$ is the separation between the surface atoms of plate II and the left surface of the dielectric medium. (See Supplementary Figs 5–7, Supplementary Table 1 and Supplementary Note 3 for more details about distance parameters.)

When the charge $Q$ on the monolayer is fixed, the total energy of the system $E(Q)$ is the sum of three parts: energy stored in the dielectric medium ($E_c$), energy of the plate II ($E^{II}$) and energy of the charged monolayer TMDs ($E^I$), as shown in Fig. 2.

$$E(Q) = E^I(Q, s^I) + E^{II}(-Q, s^{II}) + E_c$$
$$= E^I(Q, s^I) + E^{II}(-Q, s^{II}) + \frac{Q^2}{2C}, \quad (1)$$

where $C$ is the capacitance of the dielectric medium. $E^I(Q = 0, s^I)$ is the ground-state energy of the electrically neutral monolayer TMDs and $E^I(Q, s^I) - E^I(Q = 0, s^I)$ is the energy required to move electrons $Q$ from the Fermi level of the monolayer TMDs to the dielectric surface. $E^{II}(-Q, s^{II})$ is defined analogously. We take the monolayers to be undoped in this work.

The first term in equation (1), $E^I(Q, s^I)$, is calculated using DFT for each phase of the monolayer TMDs to yield a $E(Q)$ for each monolayer phase (see Supplementary Figs 1 and 2, and Supplementary Note 1 for calculation details). The phase change does not enter into the third term in equation (1) or change the capacitance of the dielectric medium $C$.

We take plate II to be a bulk metal with a work function $W$ so that the second term in equation (1) can be approximately written as:

$$E^{II}(-Q, s^{II}) = -QW. \quad (2)$$

When the voltage is fixed rather than the charge, the grand potential $\Phi_G(Q, V)$ becomes the relevant thermodynamic energy defined as:

$$\Phi_G(Q, V) = E(Q) - QV, \quad (3)$$

where $E(Q)$ is computed using equation (1). The $QV$ term in this expression represents external energy supplied to the system when the charge $Q$ flows through an externally applied voltage $V$. The equilibrium charge $Q_{eq}$ can be calculated through minimization of the grand potential at a given gate voltage $V$.

$$\left. \frac{\partial \Phi_G(Q, V)}{\partial Q} \right|_{Q=Q_{eq}} = 0 \quad (4)$$

Applying the computed $Q_{eq}(V)$ to equation (3), we can obtain the equilibrium grand potential as a function of gate voltage $\Phi_G^{eq}(V)$.

$$\Phi_G^{eq}(V) = \Phi_G(Q_{eq}(V), V) = E(Q_{eq}(V)) - Q_{eq}(V)V \quad (5)$$

Hereafter, we omit the superscript 'eq' for the equilibrium grand potential $\Phi_G^{eq}(V)$.

In addition to the electrical constraint, the nature of the mechanical constraint on the monolayer is also expected to play a role in the phase boundary, discussed in Supplementary Note 4.

**Phase boundary at constant charge.** The distinction between the constant charge and voltage cases is most important when a phase transformation occurs. We discover that the transition between semiconducting 2H-TMDs and semimetallic 1T′-TMDs can be
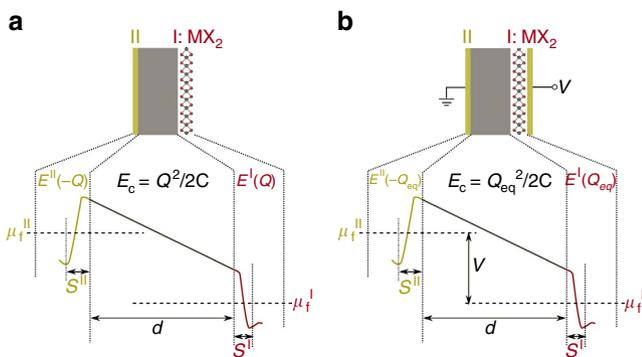


**Figure 2 | Energy calculations for systems containing a charged monolayer.** Layer I is a monolayer TMDs with a Fermi level $\mu_f^I$, and plate II has a Fermi level of $\mu_f^{II}$. Charge $Q$ on the monolayer TMDs is fixed in **a**, whereas the voltage $V$ is fixed in **b** giving rise to an equilibrium charge $Q_{eq}$. A dielectric medium of thickness $d$ and capacitance $C$, which can be vacuum, is sandwiched between the monolayer and the plate. Distance $s^I$ is the separation between the centre of the monolayer and the right surface of the dielectric medium, and $s^{II}$ is the separation between the surface atoms of plate II and left surface of the dielectric medium. The total energy in the fixed charge case is the sum of three parts: energy stored in the dielectric medium $E_c$, energy of the plate II $E^{II}$, and energy of the charged monolayer TMDs $E^I$.

driven by excess electric charge (positive or negative) in the monolayer. A constant charge condition exists when the charge on the monolayer remains constant during the phase transition as if it is electrically isolated. An approximate condition of constant charge could exist when adsorbed atoms or molecules donate charge to the monolayer.

Figure 3 presents the energy difference between the 2H and 1T′ phases as a function of the charge density in the monolayer. Figure 3a is a schematic of the system. The monolayer TMD is a distance $d$ away from the electron reservoir (metal electrode). Because the dielectric medium is vacuum in this schematic, $E^I$ and $E_c$ in equation (1) can be combined, which can be understood from Fig. 2a, and equation (1) can be rewritten as:

$$E(Q) = E^I(Q, s^I) + E^{II}(-Q, s^{II}) + E_c$$
$$= E^I(Q, s^I + d) + E^{II}(-Q, s^{II}) \qquad (6)$$

When computing the energy difference between a system where the monolayer is in the 1T′ phase and another system where the monolayer is in the 2H phase $E_{T'}(Q) - E_H(Q)$, the terms $E^{II}(-Q, s^{II})$ in equation (6) cancel, leading to,

$$E_{T'}(Q) - E_H(Q) = \left[E^I(Q, s^I + d) + E^{II}(-Q, s^{II})\right]_{T'}$$
$$- \left[E^I(Q, s^I + d) + E^{II}(-Q, s^{II})\right]_H \qquad (7)$$
$$= E_{T'}^I(Q, s^I + d) - E_H^I(Q, s^I + d)$$

Equation (7) shows that the energy difference depends on $s^I + d$ rather than $s^I$ and $d$ independently. Variation of the results of Fig. 3b,c with the separation $s^I + d$ (chosen to be 15 Å in Fig. 3) is weak or none as shown in Supplementary Fig. 7.

The blue lines are constant-stress (stress-free) cases, in which both phases exhibit minimum energy lattice constants and atomic positions. This condition is expected to hold when the monolayer is freely suspended or is not constrained by friction on a substrate. The red lines represent constant-area cases, where the monolayer is clamped to its 2H lattice constants. This condition

might be expected to hold when there is a strong frictional interaction between the monolayer and substrate preventing the monolayer from relaxing freely.

Figure 3b shows that semiconducting 2H-MoTe$_2$ has lower free energy and is the equilibrium state when the monolayer is electrically neutral or minimally charged. For the stress-free case (blue line), when the charge density is between $-0.04\,e$ and $0.09\,e$ per formula unit, 2H-MoTe$_2$ is the thermodynamically stable phase. These charge densities correspond to $-3.7 \times 10^{13}$ and $8.2 \times 10^{13}\,e\,cm^{-2}$, respectively. Outside this range, semimetallic 1T′-MoTe$_2$ will become the equilibrium phase and a transition from the semiconducting 2H phase to the semimetallic 1T′ phase will occur.

In the constant-area case (red line) in Fig. 3b, a considerably larger charge density is required to drive the phase transition. This suggests that the precise transition point may be sensitive to the presence of a substrate and that the detailed nature of the mechanical constraint of the monolayer may play a substantive role in the magnitude of the phase boundaries. The higher transition charge in this case can be understood by considering that the energy of the strained T′ phase is higher than that of the zero stress T′ phase, pushing the phase boundary to larger charge states.

Figure 3c shows that the transition in monolayer MoS$_2$ requires much larger charge density than the MoTe$_2$ case. If the negative charge density is $> 0.29\,e$ per MoS$_2$ formula unit, semimetallic 1T′-MoS$_2$ will have lower free energy and be more stable. For negative charge densities $< 0.29\,e$ per formula unit, semiconducting 2H-MoS$_2$ will be energetically favourable. This is consistent with previous experimental reports that adsorbed species donating negative charge to monolayer MoS$_2$ can trigger a trigonal prismatic to octahedral structure transformation[24,33]. MoS$_2$ single layer is reported to adopt a distorted octahedral structure when bulk MoS$_2$ is first intercalated with lithium to form Li$_x$MoS$_2$ with $x \approx 1.0$ and then exfoliated by immersion in distilled water[25]. This is qualitatively consistent with our
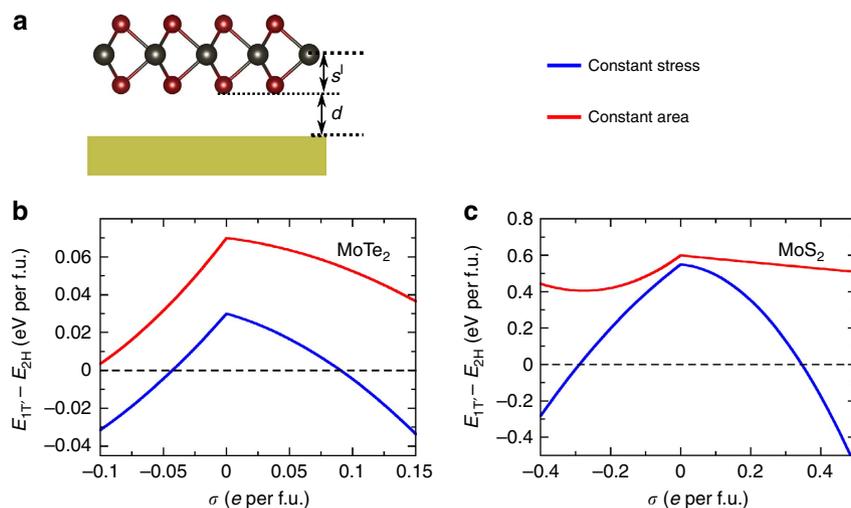


**Figure 3 | Phase boundary at constant charge in monolayer MoTe$_2$ and MoS$_2$.** (**a**) Schematic representation of a monolayer TMDs separated by vacuum from an electron reservoir, for example, the surface of a metal. The internal energy difference between 2H and 1T′ phases $E_{1T'} - E_{2H}$ changes with respect to the charge density $\sigma$ as shown in **b** and **c**. The units are per formula unit (f.u.). The blue line represents constant-stress (stress-free) case, in which both 2H and 1T′ are structure relaxed. The red line represents the constant-area case, in which the monolayer is clamped to its 2H lattice constants. (**b**) Semiconducting 2H-MoTe$_2$ is a stable phase and semimetallic 1T′-MoTe$_2$ is metastable when the monolayer is charge neutral. However, 1T′-MoTe$_2$ is more thermodynamically favourable when the monolayer is charged beyond the positive or negative threshold values. The charge thresholds exhibit a significant dependence on the relaxation of lattice constants, indicating that the precise transition point may be sensitive to the presence of a substrate. (**c**) MoS$_2$ is stable in the 2H structure when charge neutral. The magnitude of charge required for the transition to 1T′ is larger than for MoTe$_2$. In both cases, transition at constant stress is more easily induced than the transition at constant area.

prediction that a negative charge density $> 0.29\,e$ per MoS$_2$ may trigger the phase transition from 2H phase to 1T′ phase MoS$_2$. See Supplementary Fig. 8 and Supplementary Note 5 for an intuitive discussion of the mechanism for the charge-induced structural phase transition.

**Phase boundary at constant voltage.** Another relevant type of electrical constraint is fixed voltage or electron chemical potential. This constraint is most applicable when the monolayer is in an electrostatic gating structure similar to field-effect transistors made using monolayers. Such a device structure enables a dynamical approach to achieve semiconductor/semimetal phase control in monolayer TMDs, suggesting intriguing applications for ultrathin flexible 2D electronic devices including phase-change memory.

Many distinct electrostatic gating device structures can be utilized to realize this dynamic control through a change in carrier density or electron chemical potential of the monolayer. Here we consider a capacitor structure shown in Fig. 4a. A monolayer of MoTe$_2$ is deposited on top of a dielectric layer of thickness $d$, which we take to be HfO$_2$ with a large dielectric constant of 25 (ref. 34). Monolayer and dielectric are sandwiched between two metal plates between which a voltage $V$ is applied. High-dielectric constant material HfO$_2$ is chosen to increase the capacitance and hence increase the charge density in the monolayer. The metal plate is chosen to be aluminum with a work function of 4.08 eV. The curves in Fig. 4 assume the monolayer to be at a state of constant stress, with both 2H and 1T′ phases structurally relaxed. We compute the total energy and equilibrium grand potential of this system using equations (1–5).

Plotted in Fig. 4b is the total energy (equation 1) of the capacitor shown in Fig. 4a as a function of charge density in monolayer MoTe$_2$. Two black dashed lines depict common tangents between 2H and 1T′ energy surfaces, the slopes of which are defined by the set of equations,

$$\left(\frac{\partial E_H}{\partial Q}\right)_{Q_H} = \left(\frac{\partial E_{T'}}{\partial Q}\right)_{Q_{T'}} = \frac{E_H(Q_H) - E_{T'}(Q_{T'})}{Q_H - Q_{T'}} \quad (8)$$

where $V_t = \left(\frac{\partial E_H}{\partial Q}\right)_{Q_H} = \left(\frac{\partial E_{T'}}{\partial Q}\right)_{Q_{T'}}$ is the transition gate voltage.

Plotted in Fig. 4c is the equilibrium grand potential (equation 5) as a function of the gate voltage. Two transition voltages are labelled also using black dashed lines. Figure 4b,c

shows that a transition gate voltage of $-1.6$ V or 4.4 V can be applied to drive the phase transition in monolayer MoTe$_2$ using the capacitor in Fig. 4a. The experimental breakdown voltage for a 4.5-nm-thick HfO$_2$ is reported to be as large as 3.825 V (ref. 35), which is larger than twice the magnitude of the negative transition voltage. This breakdown field in HfO$_2$ is larger than some other reports and may depend on the details of growth[36,37]. Therefore, employing an appropriate dielectric is likely to be critical here in observing the phase change. Ionic liquids may be employed to help address the challenge of achieving large voltages. Ionic gating has been applied to a variety of TMDs to investigate superconductivity[38] by measuring I–V curves. However, when a large voltage is applied, it may be challenging to probe structural phase transitions from I–V curves alone due to a large density of charge in the TMDs. Structural characterization approaches, such as Raman spectroscopy, may provide a more direct probe of electrically induced structure phase transitions in monolayer TMDs.

While the curves in Fig. 4 assume that the monolayer is at a state of zero stress across the transition, Fig. 5 presents calculations for MoTe$_2$ at constant stress (Fig. 5a) and constant area (Fig. 5b) utilizing the capacitor structure shown in Fig. 4a. These phase diagrams predict the thermodynamically favoured phase as a function of voltage $V$ and thickness $d$ of the HfO$_2$ dielectric medium. In each phase diagram, there exist two phase boundaries, the positions of which vary with the work function $W$ of the capacitor plate. The 2H semiconducting phase of MoTe$_2$ is stable between the two phase boundaries, and metallic 1T′-MoTe$_2$ is stabilized by application of sufficiently positive or negative gate voltages. The transition voltages increase with the thickness of the dielectric layer. For a capacitor containing a HfO$_2$ dielectric layer of thickness $< 5$ nm, a negative gate voltage of approximately $-2$ V may be applied to drive the semiconductor-to-semimetal phase transition at constant stress (Fig. 5a) but the required voltage increases to approximately $-4$ V at constant area in Fig. 5b. In analogue with the changes in charge density phase boundaries shown in Fig. 3b, the voltage magnitudes for the transition are larger in constant-area conditions (Fig. 5b) than at constant stress (Fig. 5a). If the substrate constrains the area of the monolayer across the transition through friction, the voltages in Fig. 5b are expected to be applicable. The figure also shows a reported experimental breakdown voltage of a 4.5-nm-thick HfO$_2$ film[35].

Field-effect transistors based on few-layered MoTe$_2$ have been reported in ref. 39 using a 270-nm-thick SiO$_2$ gate dielectric layer
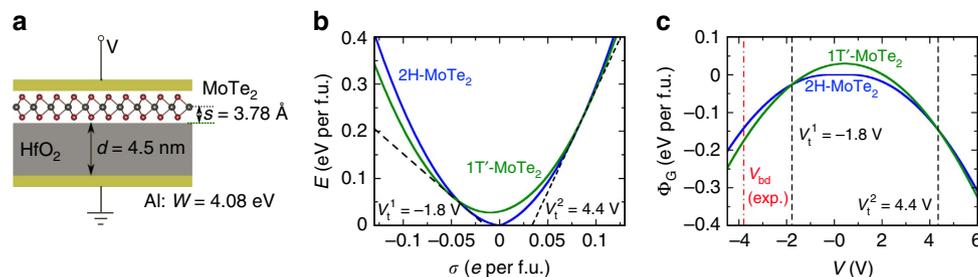


**Figure 4 | Phase boundary at constant voltage and stress.** (**a**) Monolayer MoTe$_2$ deposited on top of a HfO$_2$ layer of thickness $d = 4.5$ nm, which is on top of an aluminum plate of work function $W = 4.08$ eV. Voltage $V$ is applied between the monolayer and the aluminum plate. (**b**) Plotted is the total energy $E$ of the capacitor shown in **a** as a function of the charge density $\sigma$ on monolayer MoTe$_2$. (**c**) Plotted is the grand potential $\Phi_G$ as a function of the gate voltage $V$. The blue line represents a capacitor containing 2H-MoTe$_2$, whereas the green line represents a capacitor containing 1T′-MoTe$_2$. The two black dashed lines in **b** depict common tangents between the 2H and 1T′ energy surfaces, and in **c** represent intersections of the 2H and 1T′ grand potentials indicating two transition voltages $V_t^1$ and $V_t^2$. Between the two transition voltages, semiconducting 2H-MoTe$_2$ has a lower grand potential and is thermodynamically stable. Outside this range, 1T′ will be more stable. The red dashed line in **c** represents a breakdown voltage[35] obtained experimentally for a HfO$_2$ film of thickness 4.5 nm. The separation between MoTe$_2$ centre and the surface of HfO$_2$ is assumed to be $s = 3.78$ Å, and both 2H and 1T′ are structurally relaxed (constant stress) in **b** and **c**.
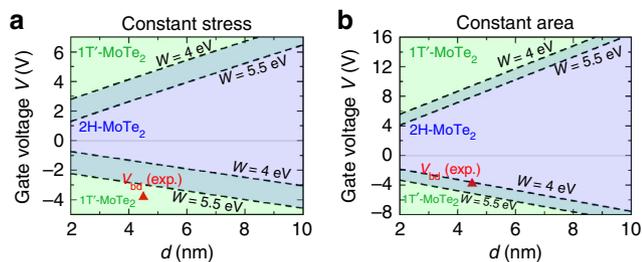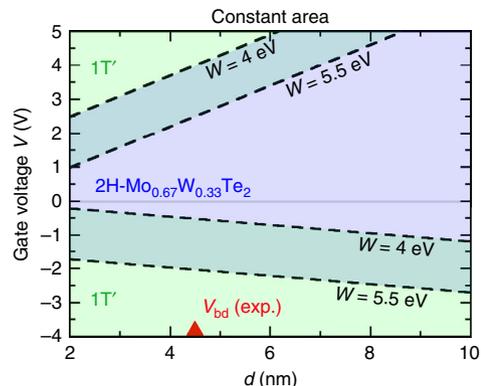
**Figure 5 | Phase control of MoTe₂ through gating at constant stress and constant area.** (**a,b**) Plotted are phase stabilities of monolayer MoTe₂ with respect to gate voltage $V$ and dielectric thickness $d$ using the capacitor structure shown in Fig. 4a. In each phase diagram, there exist two phase boundaries that vary with the work function $W$ of the capacitor plate. Between the two phase boundaries, semiconducting 2H is more stable, and outside 1T′ is the stable structure. The required transition gate voltage is smaller in the constant-stress case (**a**) than in the constant-area case (**b**). For a constant-stress scenario, a negative gate voltage as small as $-1$ to $-2$ V can trigger the semiconducting-to-semimetallic phase transition in monolayer MoTe₂. The red triangle represents the breakdown voltage of a 4.5-nm-thick HfO₂ film obtained experimentally[35].



**Figure 6 | Reducing transition gate voltages with the alloy $Mo_xW_{1-x}Te_2$.** Plotted is the phase stability of a representative alloyed monolayer $Mo_{0.67}W_{0.33}Te_2$ with respect to the gate voltage $V$ and the dielectric thickness $d$ using the capacitor structure as shown in Fig. 4a. The transition is assumed to occur at constant monolayer area. The magnitudes of the transition gate voltages in this alloy are smaller than those of pure MoTe₂ monolayer indicating the potential for phase boundary engineering.

(3.9 dielectric constant) with gate voltages as large as $-50$ V. For monolayer MoTe₂ (rather than few layers), our model predicts that a gate voltage $>200$ V is required to drive the phase transition for this device configuration. Both the increase of dielectric thickness (from 5 to 270 nm) and the decrease of dielectric constant (from 25 for HfO₂ to 3.9 for SiO₂ (ref. 35)) will result in larger transition gate voltages than shown in Fig. 5. To observe the 2H-1T′ phase transition in a device, choosing a dielectric medium of large dielectric constant and dielectric performance will be critical.

**Reducing transition gate voltages with the alloy $Mo_xW_{1-x}Te_2$.** Monolayer alloys present the possibility for reducing the required gate voltage by varying the chemical composition. Recently, monolayer alloys of Mo- and W-dichalcogenides have attracted increasing attention for their tunable properties[40–44]. We hypothesize that the 2H-1T′ transition gate voltage can be tuned to lower values by alloying MoTe₂-WTe₂ monolayers. This is because in monolayer MoTe₂, the 2H phase is energetically favourable by 31 meV per formula unit relative to the 1T′ phase, whereas in monolayer WTe₂, the energy of the 1T′ phase is 123 meV per formula lower than the 2H phase, as shown in Supplementary Fig. 4. Therefore, one might expect the energy difference between the two charge-neutral phases to be tunable through zero with alloy composition. The smaller the energy difference is, the closer the phase boundary is to ambient condition and the smaller the external force required to drive the phase transition in monolayer TMDs[20]. Therefore, controlling alloy composition is likely to enable tuning of the transition gate voltage.

Earlier experimental reports of the synthesis of the bulk alloy $Mo_xW_{1-x}Te_2$ (ref. 45) and detailed calculations on monolayers[44] indicate that the phase changes from 2H to 1T′ with increase in W fraction $1-x$. This indicates that the free energy difference between the 2H and 1T′ phases can be made arbitrarily small by varying $x$, enabling an arbitrary reduction of the gate voltage. However, the precise value of $x$ required to achieve a particular transition voltage is likely to depend on a number of factors including synthesis conditions and mechanical constraints[44,45]. Here we study an approximate representative atomic configuration for this alloy for $x=0.67$, displayed in Supplementary Fig. 9, with the knowledge that some variation of

computed phase diagram can occur with the choice of configuration. Detailed cluster expansion calculations for these monolayer alloys are presented in ref. 44.

For the alloy configuration we employed in this work (assumed at constant area), the 2H phase is a semiconductor with a semilocal quasiparticle Kohn–Sham bandgap of $\sim 0.9$ eV, and its free energy is 15 meV lower than the 1T′ phase at constant monolayer area, which is metallic or semimetallic. Figure 6 shows that the 2H-1T′ phase transition in this alloy can be driven by negative gating of a smaller gate voltage than pure MoTe₂ monolayer. For example, assuming HfO₂ medium of 4.5-nm thickness and capacitor plate of 4.0 eV work function, the magnitude of negative transition gate voltage can be reduced from 3.6 V (MoTe₂, constant-area case) to 0.4 V in the constant-area case of $Mo_{0.67}W_{0.33}Te_2$ monolayer.

One might expect that the transition gate voltage in monolayers can be tuned and reduced potentially arbitrarily by controlling the chemical composition of this and other potentially alloys. To enable a structural phase transition driven by a small gate voltage, elements should be selected for alloying so that the energy difference between charge-neutral 2H and 1T′ phases can be tuned through zero with alloy composition. Alternative mechanical constraints placed on the alloy monolayer (for example, constant stress) can also be expected to shift the phase boundary and transition gate voltage.

**Phase transition in Ta-based TMDs.** Electrically induced structural phase changes between 2H and 1T phases in the Ta-based TMDs, TaSe₂ and TaS₂, have been reported in experiments using a STM tip[17,18], although the mechanism for this reported effect may differ from the charge-induced effect reported in the present work. As a supplement to the previous calculations on group VI TMDs, we have computed the constant-stress phase diagram of monolayer TaSe₂ in the capacitor gating structure shown in Fig. 7a. Figure 7b shows that the phase diagram of TaSe₂ has a phase boundary at only positive gate voltage, qualitatively different from MoTe₂ and MoS₂. We find that this difference results from the metallic nature of both 2H- and 1T-TaSe₂, further discussed in Supplementary Note 5.

A qualitative difference between these calculations and the STM experiment[17] is the observation of the transition at both signs of STM bias, suggesting that other effects could be at play in the experiment. Further quantitative comparison with the
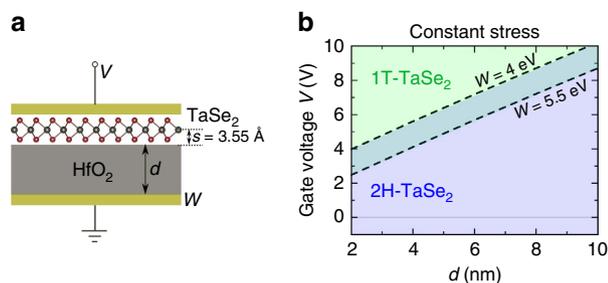
**Figure 7 | Phase control of monolayer TaSe$_2$ through gating at constant stress.** (**b**) Plotted is the computed phase diagram of monolayer TaSe$_2$ in the capacitor gating structure as shown in **a**. Unlike MoTe$_2$, the phase diagram of TaSe$_2$ only has one phase boundary, which corresponds to a positive gate voltage. Below the phase boundary, 2H-TaSe$_2$ is more stable; above the boundary, 1T has lower energy and is more stable. Intuition for this qualitative difference from MoTe$_2$ is provided in Supplementary Note 5.

experiment is made challenging by the small separation between the monolayer and the STM tip (Supplementary Fig. 3; Supplementary Note 2).

## Discussion

The electrical dynamical control of structural phase in monolayer TMDs has exciting potential applications in ultrathin flexible 2D electronic devices. If the kinetics of the transformation are suitable, nonvolatile phase-change memory[9] may be an application. One might expect 2D materials to have energy consumption advantages over bulk materials due to their small thickness. If the kinetics is sufficiently fast, another potential application may be subthreshold swing reduction in field-effect transistors to overcome the scaling limit of conventional transistors[4]. In addition, the change in the transmittance of light due to the phase transition of monolayer TMDs may be employed in infrared optical switching devices, such as infrared optical shutters and modulators for cameras, window coating and infrared antennas with tunable resonance.

To summarize, we have identified a new mechanism, electrostatic gating, to induce a structural semiconductor-to-semimetal phase transition in monolayer TMDs. We have computed phase boundaries for monolayer MoTe$_2$, MoS$_2$ and TaSe$_2$. We discover that changing carrier density or electron chemical potential in the monolayer can induce a semiconductor-to-semimetal phase transition in monolayer TMDs. We find that a surface charge density less than $-0.04e$ or greater than $0.09e$ per formula unit is required to observe the semiconductor-to-semimetal phase transition in monolayer MoTe$_2$ under constant-stress conditions, and a significantly larger value of approximately $-0.29e$ or $0.35e$ per formula unit is required in the monolayer MoS$_2$ case. A capacitor structure can be employed to dynamically control the semiconductor-to-semimetal phase transition in monolayer MoTe$_2$ with a gate voltage $\sim 2$–$4$ V for MoTe$_2$. These transition charges and voltages are expected to vary considerably with the nature of the mechanical constraint of the monolayer and also potentially the presence of dopants or Fermi level pinning. While the gate voltages required to observe the transition in MoTe$_2$ are likely near breakdown and could be challenging to realize in the lab, we find that the voltage magnitudes can be reduced arbitrarily by alloying Mo atoms with substitutional W atoms to create the alloy Mo$_x$W$_{1-x}$Te$_2$.

## Methods

**Electronic structure calculations.** All periodic DFT calculations were performed within the Vienna Ab Initio Simulation Package[46], version 5.3.3, using the

projector augmented-wave[47] method and the plane-wave basis set with a kinetic energy cutoff of 350 eV. Electron exchange and correlation effects were treated using the Generalized Gradient Approximation (GGA) functional of Perdew, Burke and Ernzerhof[48]. An $18 \times 18 \times 1$ Monkhorst-Pack[49] k-point mesh was utilized to sample the Brillouin zone. The convergence thresholds for electronic and ionic relaxations were chosen to be $0.5 \times 10^{-8}$ eV per MX$_2$ formula unit and $0.5 \times 10^{-7}$ eV per MX$_2$ formula unit, respectively. A Gaussian smearing of 50 meV was used. The computational cell length is 36 Å along the $c$ axis. Spin–orbit coupling is employed in all DFT calculations. The ionic relaxations were performed using conjugate gradient algorithm.

All calculations in this work were performed at zero ionic temperature, omitting the vibrational component of the free energy. Reference 20 has shown that inclusion of vibrational free energy and temperature would shift the phase boundaries closer to ambient conditions and lower the energy required to switch the phases. Therefore, one would expect inclusion of these effects to decrease the magnitude of the transition charge density and gate voltage calculated in this work. Also, the change of bandgap width is expected to affect 2H-1T′ phase boundary, as further discussed in Supplementary Fig. 10 and Supplementary Note 6. See Supplementary Note 7 for a discussion on vacuum electronic states.

## References

1. Lencer, D. *et al.* A map for phase-change materials. *Nat. Mater.* **7**, 972–977 (2008).
2. Wong, H.-S. P. *et al.* Phase change memory. *Proc. IEEE* **98**, 2201–2227 (2010).
3. Wong, H.-S. P. *et al.* Metal-oxide RRAM. *Proc. IEEE* **100**, 1951–1970 (2012).
4. Zhou, Y. & Ramanathan, S. Correlated electron materials and field effect transistors for logic: a review. *Crit. Rev. Solid State Mater. Sci.* **38**, 286–317 (2013).
5. Shu, M. J. *et al.* Ultrafast terahertz-induced response of GeSbTe phase-change materials. *Appl. Phys. Lett.* **104**, 251907 (2014).
6. Aetukuri, N. B. *et al.* Control of the metal-insulator transition in vanadium dioxide by modifying orbital occupancy. *Nat. Phys.* **9**, 661–666 (2013).
7. Cavalleri, A. *et al.* Femtosecond structural dynamics in VO$_2$ during an ultrafast solid-solid phase transition. *Phys. Rev. Lett.* **87**, 237401 (2001).
8. Kikuzuki, T. & Lippmaa, M. Characterizing a strain-driven phase transition in VO2. *Appl. Phys. Lett.* **96**, 132107 (2010).
9. Wuttig, M. & Yamada, N. Phase-change materials for rewriteable data storage. *Nat. Mater.* **6**, 824–832 (2007).
10. Lee, S.-H., Jung, Y. & Agarwal, R. Highly scalable non-volatile and ultra-low-power phase-change nanowire memory. *Nat. Nanotechnol.* **2**, 626–630 (2007).
11. Bulaevskiĭ, L. N. Structural transitions with formation of charge-density waves in layer compounds. *Sov. Phys. Uspekhi* **19**, 836–843 (1976).
12. McMillan, W. L. Theory of discommensurations and the commensurate-incommensurate charge-density-wave phase transition. *Phys. Rev. B* **14**, 1496–1502 (1976).
13. Thomson, R. E., Burk, B., Zettl, A. & Clarke, J. Scanning tunneling microscopy of the charge-density-wave structure in 1T-TaS$_2$. *Phys. Rev. B* **49**, 16899–16916 (1994).
14. Scruby, C. B., Williams, P. M. & Parry, G. S. The role of charge density waves in structural transformations of 1T TaS$_2$. *Philos. Mag.* **31**, 255–274 (1975).
15. Castro Neto, A. H. Charge density wave, superconductivity, and anomalous metallic behavior in 2D transition metal dichalcogenides. *Phys. Rev. Lett.* **86**, 4382–4385 (2001).
16. Wilson, J. A. & Yoffe, A. D. The transition metal dichalcogenides discussion and interpretation of the observed optical, electrical and structural properties. *Adv. Phys.* **18**, 193–335 (1969).
17. Zhang, J., Liu, J., Huang, J. L., Kim, P. & Lieber, C. M. Creation of nanocrystals through a solid-solid phase transition induced by an STM tip. *Science* **274**, 757–760 (1996).
18. Kim, J.-J. *et al.* Observation of a phase transition from the T phase to the H phase induced by a STM tip in 1T-TaS$_2$. *Phys. Rev. B* **56**, R15573–R15576 (1997).
19. Mak, K. F., Lee, C., Hone, J., Shan, J. & Heinz, T. F. Atomically thin MoS$_2$: a new direct-gap semiconductor. *Phys. Rev. Lett.* **105**, 136805 (2010).
20. Duerloo, K.-A. N., Li, Y. & Reed, E. J. Structural phase transitions in two-dimensional Mo- and W-dichalcogenide monolayers. *Nat. Commun.* **5**, 4214 (2014).
21. Eda, G. *et al.* Coherent atomic and electronic heterostructures of single-layer MoS$_2$. *ACS Nano* **6**, 7311–7317 (2012).
22. Gao, G. *et al.* Charge mediated semiconducting-to-metallic phase transition in molybdenum disulfide monolayer and hydrogen evolution reaction in new 1T′ phase. *J. Phys. Chem. C* **119**, 13124–13128 (2015).
23. Kan, M. *et al.* Structures and phase transition of a MoS$_2$ monolayer. *J. Phys. Chem. C* **118**, 1515–1522 (2014).
24. Kang, Y. *et al.* Plasmonic hot electron induced structural phase transition in a MoS$_2$ monolayer. *Adv. Mater.* **26**, 6467–6471 (2014).

25. Jiménez Sandoval, S., Yang, D., Frindt, R. F. & Irwin, J. C. Raman study and lattice dynamics of single molecular layers of $MoS_2$. *Phys. Rev. B* **44,** 3955–3962 (1991).

26. Kan, M., Nam, H. G., Lee, Y. H. & Sun, Q. Phase stability and Raman vibration of the molybdenum ditelluride ($MoTe_2$) monolayer. *Phys. Chem. Chem. Phys.* **17,** 14866–14871 (2015).

27. Wang, Q. H., Kalantar-Zadeh, K., Kis, A., Coleman, J. N. & Strano, M. S. Electronics and optoelectronics of two-dimensional transition metal dichalcogenides. *Nat. Nanotechnol.* **7,** 699–712 (2012).

28. Radisavljevic, B., Radenovic, A., Brivio, J., Giacometti, V. & Kis, A. Single-layer $MoS_2$ transistors. *Nat. Nanotechnol.* **6,** 147–150 (2011).

29. Brown, B. E. The crystal structures of $WTe_2$ and high-temperature $MoTe_2$. *Acta Crystallogr.* **20,** 268–274 (1966).

30. Keum, D. H. *et al.* Bandgap opening in few-layered monoclinic $MoTe_2$. *Nat. Phys.* **11,** 482–486 (2015).

31. Ruppert, C., Aslan, O. B. & Heinz, T. F. Optical properties and band gap of single- and few-layer $MoTe_2$ crystals. *Nano Lett.* **14,** 6231–6236 (2014).

32. Lezama, I. G. *et al.* Indirect-to-direct band gap crossover in few-layer $MoTe_2$. *Nano Lett.* **15,** 2336–2342 (2015).

33. Lin, Y.-C., Dumcenco, D. O., Huang, Y.-S. & Suenaga, K. Atomic mechanism of the semiconducting-to-metallic phase transition in single-layered $MoS_2$. *Nat. Nanotechnol.* **9,** 391–396 (2014).

34. Ray, S. K., Mahapatra, R. & Maikap, S. High-k gate oxide for silicon hetero-structure MOSFET devices. *J. Mater. Sci. Mater. Electron* **17,** 689–710 (2006).

35. Kang, L. *et al.* Electrical characteristics of highly reliable ultrathin hafnium oxide gate dielectric. *IEEE Electron Device Lett.* **21,** 181–183 (2000).

36. Lee, J.-H. *et al.* Characteristics of ultrathin HfO2 gate dielectrics on strained-Si0.74Ge0.26 layers. *Appl. Phys. Lett.* **83,** 779–781 (2003).

37. Wolborski, M., Rooth, M., Bakowski, M. & Hallén, A. Characterization of HfO2 films deposited on 4H-SiC by atomic layer deposition. *J. Appl. Phys.* **101,** 124105 (2007).

38. Shi, W. *et al.* Superconductivity series in transition metal dichalcogenides by ionic gating. *Sci. Rep.* **5,** 12534 (2015).

39. Pradhan, N. R. *et al.* Field-effect transistors based on few-layered α-$MoTe_2$. *ACS Nano* **8,** 5911–5920 (2014).

40. Chen, Y. *et al.* Tunable band gap photoluminescence from atomically thin transition-metal dichalcogenide alloys. *ACS Nano* **7,** 4610–4616 (2013).

41. Zhang, M. *et al.* Two-dimensional molybdenum tungsten diselenide alloys: photoluminescence, Raman scattering, and electrical transport. *ACS Nano* **8,** 7130–7137 (2014).

42. Kutana, A., Penev, E. S. & Yakobson, B. I. Engineering electronic properties of layered transition-metal dichalcogenide compounds through alloying. *Nanoscale* **6,** 5820–5825 (2014).

43. Tongay, S. *et al.* Two-dimensional semiconductor alloys: Monolayer Mo1-xWxSe2. *Appl. Phys. Lett.* **104,** 012101 (2014).

44. Duerloo, K.-A. N. & Reed, E. J. Structural phase transitions by design in monolayer alloys. *ACS Nano.* doi: 10.1021/acsnano.5b04359 (2015).

45. Champion, J. A. Some properties of (Mo, W) (Se, Te) 2. *Br. J. Appl. Phys.* **16,** 1035 (1965).

46. Kresse, G. & Furthmüller, J. Efficient iterative schemes for ab initio total-energy calculations using a plane-wave basis set. *Phys. Rev. B* **54,** 11169–11186 (1996).

47. Blöchl, P. E. Projector augmented-wave method. *Phys. Rev. B* **50,** 17953–17979 (1994).

48. Perdew, J. P., Burke, K. & Ernzerhof, M. Generalized gradient approximation made simple. *Phys. Rev. Lett.* **77,** 3865–3868 (1996).

49. Monkhorst, H. J. & Pack, J. D. Special points for Brillouin-zone integrations. *Phys. Rev. B* **13,** 5188–5192 (1976).

## Author contributions
Y.L., K-A.N.D. and E.J.R. designed the simulations and the framework for thermodynamic analysis; Y.L. performed the simulations and subsequent numerical data analysis; Y.L. and K.W. performed the preliminary simulations. Y.L. and E.J.R. interpreted the data and wrote the paper.

## Additional information
**Supplementary Information** accompanies this paper at http://www.nature.com/naturecommunications

**Competing financial interests:** The authors declare no competing financial interests.

**Reprints and permission** information is available online at http://npg.nature.com/reprintsandpermissions/

**How to cite this article:** Li, Y. *et al.* Structural semiconductor-to-semimetal phase transition in two-dimensional materials induced by electrostatic gating. *Nat. Commun.* 7:10671 doi: 10.1038/ncomms10671 (2016).